Article Type: Original Article

Regulated Cell Death of Lymphoma Cells after Graded Mitochondrial Damage is differentially affected by Drugs Targeting Cell Stress Responses

Tomás Lombardo [a], Martín Gil Folgar [a], Luciana Salaverry [b], Estela Rey-Roldán [b], Elida M. Alvarez [c], María C Carreras [d], Laura Kornblihtt [e] and Guillermo A. Blanco [a]

[a] Laboratory of Immunotoxicology (LaITo), IDEHU-CONICET, Clinics Hospital, José de San Martín, University of Buenos Aires (UBA), Buenos Aires, Argentina

[b] Laboratory of Reproductive Immunology (LAIR) IDEHU-CONICET, Faculty of Pharmacy and Biochemistry, UBA, Buenos Aires, Argentina

[c] Laboratory of Tumour Immunology (LIT), IDEHU-CONICET, Faculty of Pharmacy and Biochemistry, UBA, Buenos Aires, Argentina

[d] Laboratory of Oxygen Metabolism, University of Buenos Aires, INIGEM-CONICET, Argentina

[e] Haematology Department, Clinics Hospital, José de San Martín, University of Buenos Aires (UBA), Buenos Aires, Argentina

(Received 20 October 2017; Accepted 26 November 2017)

Author for correspondence: Guillermo A. Blanco, Laboratorio de Inmunotoxicología (LaITo), IDEHU - CONICET – UBA, Junin 956 4to piso, Capital Federal (1113), Argentina (e-mail: gblanco@ffyb.uba.ar).

Running title: Survival of lymphoma cells after graded mitochondrial damage

Keywords

Mitophagy; Mitochondrial fission; Mdivi-1; Lysosomes; valproic acid; Lymphoma

Abbreviations

CCCP, Carbonyl cyanide 3-chlorophenylhydrazone; Mdivi-1, 3-(2,4-Dichloro-5-methoxyphenyl)-2,3-dihydro-2-thioxo-4(1H)-quinazolinone; IAA, iodoacetamide; VCR, Vincristine; VPA, Valproic acid; FDA, Fluorescein-diacetate; TMRE, Tetramethylrhodamine-ethyl-ester, NAO, Nonyl-acridine orange; HE, hydroethidine; 5CMF, 5-chloromethylfluorescein diacetato; PI, propidium iodide; MTKred, MitoTrackerR Red; MDC, monodancyl-cadaverine

Abstract: Collapse of the mitochondrial membrane potential (MMP) is often considered the initiation of regulated cell death (RCD). Carbonyl cyanide 3-chlorophenylhydrazone (CCCP) is an uncoupler of the electron transport chain (ETC) that facilitates the translocation of protons into the mitochondrial matrix leading to the collapse of the MMP. Several cell stress responses such as mitophagy, mitochondrial biogenesis and the ubiquitin proteasome system, may differentially contribute to restrain the initiation of RCD depending on the extent of mitochondrial damage. We induced graded mitochondrial damage after collapse of MMP with the mitochondrial uncoupler CCCP in Burkitt's lymphoma cells, and we evaluated the effect of several drugs targeting cell stress responses over RCD at 72 hr, using a multiparametric flow cytometry approach. CCCP caused collapse of MMP after 30 min., massive mitochondrial fission, oxidative stress and increased mitophagy within the 5-15 μM low-dose range (LDR) of CCCP. Within the 20-50 μM high-dose range (HDR), CCCP caused lysosomal destabilization and rupture, thus precluding mitophagy and autophagy. Cell death after 72 hr was below 20%, with increased mitochondrial mass (MM). The inhibitors of mitophagy Mdivi-1 and vincristine increased cell death from CCCP within the LDR, while valproic acid (an inducer of mitochondrial biogenesis) also increased MM and cell death within the LDR. The proteasome inhibitor, MG132, increased cell death only in the HDR. Doxycycline, an antibiotic that disrupts mitochondrial biogenesis, had no effect on cell survival, while iodoacetamide, an inhibitor of glycolysis, increased cell death at the HDR. We conclude that mitophagy influenced RCD of lymphoma cells after MMP collapse by CCCP only within the LDR, while proteasome activity and glycolysis contributed to survival in the HDR under extensive mitochondria and lysosome damage.

Regulated cell death (RCD) involves an active form of cell suicide that occurs when homeostatic cell stress responses are overwhelmed under cell damage, such as that caused by cytotoxic drugs [1]. The initiation of mitochondrial apoptosis may occur in situations where drugs directly elicit cytotoxic effector pathways, or when they block pro-survival cells stress responses [2]. Massive collapse of mitochondrial membrane potential (MMP) is often considered the initial step of mitochondrial apoptosis, also known as intrinsic apoptosis [3]. This is due to increased mitochondrial reactive oxygen species (ROS) and extensive mitochondrial damage after collapse of MMP [4]. Increased mitochondrial ROS leads to oxidation of cardiolipin (CL), release of cytochrome c from mitochondria, formation of the apoptosome and activation of caspases, among many other molecular events [5]. Several pharmacological compounds used in the treatment of leukaemia and lymphomas, including arsenic, fludarabine and anti-CD20, are known to initiate mitochondrial apoptosis [6]. Carbonyl cyanide 3-chlorophenylhydrazone (CCCP) is an uncoupler of the electron transport chain (ETC). Uncouplers are small molecules that allow the movement of protons into the mitochondrial matrix following their electrochemical gradient, leading to the collapse of the MMP, increased mitochondrial ROS and progressive mitochondrial failure that leads to apoptosis [7]. Several cytotoxic drugs share this initial step of mitochondrial apoptosis and the term "mitocans" has been proposed to refer to drugs with anti-cancer activity that induce apoptosis by destabilizing the mitochondria [6]. The therapeutic margin of CCCP and other classical uncouplers is relatively narrow for clinical use, and a new generation of uncouplers aims to overcome this obstacle [8]. However, the study of cell stress responses opposing the effect of uncouplers may be relevant to the understanding of the mechanisms of resistance to other mitocans. Mitochondrial damage initiates a broad spectrum of stress responses that are often enhanced in tumour cells. Therefore, these cells may be able to bypass the initiation of apoptosis and survive even with massive collapse of MMP [9, 10]. Mitophagy has been proposed as one of the stress responses that aids to eliminate damaged mitochondria and prevent the initiation of apoptosis [11]. Externalization of mitochondrial CL can operate as an “eat-me” signal at the initiation of mitophagy [12]. Enhanced mitophagy in lymphoma and leukaemia cells can be an important factor contributing to pharmacological resistance to cytotoxic drugs [13]. Mitophagy requires fission of mitochondria, and compounds that prevent fission, such as Mdivi-1, may hamper mitophagy at its very early step [14]. Inhibitors of the microtubule network such as vincristine (VCR), widely used in drug combinations in the treatment of leukaemia and lymphoma, can block mitophagy by preventing the transport and delivery of mitophagosomes to lysosomes, the organelle where eventual elimination takes place [10, 13, 15]. Mitochondrial biogenesis may contribute to cell survival after drug-induced mitochondrial damage [16]. In that sense, mitochondrial biogenesis may be seen as a stress response in itself, completing a

cycle of mitochondrial turnover [17]. Valproic acid is known to increase mitochondrial biogenesis and could aid some tumour cells to survive [13, 18]. However, the increase in mitochondrial mass may be harmful in conditions of persistent mitochondrial damage [19]. Finally, the metabolic crisis due to massive mitochondrial damage may create a temporal dependence on glycolysis as a source of energy for cell survival [20].

In this study, we evaluated the influence of drugs targeting cell stress responses on survival rates at 72 hr, after incremental mitochondrial damage inflicted by CCCP treatment on Burkitt's lymphoma cells. We found that at low CCCP doses, mitophagy actively contributed to cell survival, but at higher doses mitophagy was no longer possible due to complete destabilization and rupture of lysosomes.

Materials and Methods

1- Reagents, cell line and culture conditions

Carbonyl cyanide 3-chlorophenylhydrazone (CCCP) and 3-(2,4-Dichloro-5-methoxyphenyl)-2,3-dihydro-2-thioxo-4(1H)-quinazolinone (Mdivi-1) were from Sigma (Buenos Aires, Argentina). Stock solutions were prepared in dimethylsulfoxide (DMSO) at 80 mM and 5 mM concentration, respectively. The maximal final concentration of DMSO used in samples were 0.06% and 1%, respectively. MG-132 was obtained from Calbiochem (San Diego, CA, USA) and prepared as 5mM stock solutions. Valproic acid was from Casasco Pharmaceuticals (Argentina) and was prepared freshly as a 100-mM stock solution in RPMI-1640. Doxycycline was from Pfizer Pharmaceuticals (Argentina) and was prepared freshly as a 20-mM stock solution in phosphate buffer saline (PBS). Vincristine was kindly provided by Laboratorio Filaxis (Argentina). RPMI-1640, penicillin, streptomycin, fluorescein-diacetate (FDA), tetramethylrhodamine-ethyl-ester (TMRE), Nonyl-acridine orange (NAO), hydroethidine (HE), 5-chloromethylfluorescein diacetate (5CMF), propidium iodide (PI) and MitoTrackerR Red (MTKred) were purchased from ThermoFisher. Raji cells were purchased from ATCC and grown in RPMI 1640 with 10% foetal bovine serum (FBS) at 37°C in a 5% CO_2 atmosphere. Cells were subcultured at 1:2 ratios every 2 to 3 days in 75 cm2 culture flasks (Corning) with a viability greater than 95%. For the experimental assessment of drugs, Raji cells were decanted in 24-well culture plates at 0.5 x 10^6/ml. Serial dilutions of CCCP, or drug combinations were added in triplicate. RPMI was added as untreated control. The final volume of media in the 24-well plate for each culture sample was 1ml. The plates were incubated for 30 min. or 72 hr at 37°C with 5% CO_2.

2- Labelling of cells with fluorescent probes for fluorescence microscopy and flow cytometry

Nonyl-acridine orange (NAO), a green fluorescent probe that binds to cardiolipin (CL), was used to estimate mitochondrial mass (MM) by flow cytometry [13]. NAO emits low fluorescence when bound to oxidized CL (oxCL) and high fluorescence when bound to non-oxidized normal CL (rdCL) in the internal mitochondrial membrane [21, 22]. NAO was prepared as a 5-mM stock solution in ethanol, and diluted to 100 nM in PBS to stain cells during 15 min. at 37°C. The cells were washed once in PBS and analysed by flow cytometry or fluorescence microscopy.

For observation of lysosomes, Raji cells were stained first with 20 µM acridine orange (AO; from Sigma) for 10 min., washed in PBS and pelleted before mounting onto slides for live observation under fluorescence microscopy. AO becomes highly concentrated in acid vesicles and emits red fluorescence due to spectral shift [23].

For observation of autophagosomes, cells were stained with 50 µM monodancyl-cadaverine (MDC; from Sigma) in RPMI at 37°C during 10 min. and evaluated by flow cytometry or fluorescence microscopy [13]. For double-stained assays in fluorescence microscopy, cells were first stained with AO as described above and then labelled with MDC for 10 min. Observation of autophagolysosomes by red fluorescence after UV-light excitation was done at least 20 min. after labelling with MDC, to allow this probe that loads into autophagosomes to partially reach the lysosomes and mix with AO, which is highly concentrated in lysosomes. The coincidence of MDC and AO in lysosomes created a donor-acceptor interaction that produced red fluorescence emission with UV excitation in autophagolysosomes. We used MTKred as an alternative fluorescent marker for mitochondria in fluorescence microscopy assays. A stock solution of 1 mM MTKred was prepared in DMSO and further used to label cells by suspending them at a final concentration of 50 nM during 20 min. at 37°C in PBS (final concentration of DMSO below 0.01%), then washed once in PBS and mounted onto slides for microscopic observation. Superoxide anion ($O_2^{\cdot-}$) was evaluated with hydroethidine (HE), a probe that is oxidized to ethidium by intracellular $O_2^{\cdot-}$, and glutathione (GSH) levels were detected with 5-chloromethylfluorescein diacetate (5CMF), a probe that forms fluorescent-adducts with intracellular non-protein thiols [24]. Staining with 1 µM fluorescein-diacetate (FDA) and 1 µM PI was also conducted to obtain a comparative score of dead cells by flow cytometry [24, 25]. In addition, FDA was used as a probe for intracellular pH for monitoring changes after 30-min. treatment with CCCP [26].

3- Multiparametric flow cytometry assessment of MM, MMP, autophagosomes and cell death

We employed a flow cytometry multiparametric method to simultaneously assess mitochondrial mass (MM), mitochondrial membrane potential (MMP), cell death and the amount of autophagosomes in single cells. The MMP was evaluated by the potentiometric probe TMRE [13]. Cells were incubated in 0.05 µM TMRE for 20 min. at 37°C. The MM was evaluated with NAO, cell death was evaluated with 1 µM PI and autophagosomes were evaluated with 50 µM MDC.

4- Cellular and subcellular flow cytometry analysis

All samples were evaluated in a Partec PAS III flow cytometer equipped with a 20 mW 488nm argon blue laser and a 100 W UV lamp (Partec, GmbH, Münster, Germany). A total of 20,000 cells were analysed in each sample. Fluorescence from NAO, FDA and 5CMF was collected through a 520/10 nm bandpath (BP) filter (FL1). Fluorescence from TMRE and HE was collected with a 590/20 nm BP filter (FL2) and PI was collected with 670/20 nm BP filter. MDC was the only probe excited with UV-light 340/30 nm in a separate illumination point and collected with a 455/10 nm BP filter (FL6).

For subcellular flow cytometry analysis, samples were stained with NAO and PI as described above, sonicated for 2 min. at 30kHz and immediately run in the flow cytometer [10, 27]. Acquisition was restricted to mitochondria-containing particles by using NAO fluorescence threshold as the input criteria. A total of 40,000 mitochondria-containing particles were analysed in each sample. Forward-scattered light (FSC) and side-scattered light (SSC) parameters were acquired in log scale. The area and width of the pulses of SSC and FSC (SSC-A ,SSC-W, FSC-A and FSC-W, respectively) were recorded and used for the analysis of shape changes in mitochondria-containing particles after CCCP treatment. Flow cytometry data analysis was performed with Flomax software (Partec, Germany) and WinMDI 2.8 (Scripps Research Institute, USA).

5- Light and fluorescence microscopy

Slide preparations were observed in an Olympus BX-51 fluorescence microscope equipped with a 100 Watt mercury lamp, a halogen lamp for transmitted light, U-plan fluorite objectives and three fluorescence filter cubes (U-MWU2, U-MWB2 and U-MWG2 for ultraviolet, blue and green excitation light, respectively). All images were acquired with a digital Q-Color 3 Olympus camera and Image-Pro Plus 6.0 software (Media Cybernetics, USA). Image processing was performed with Image-Pro Plus 6.0. MDC fluorescence (cyan) and FRET (fluorescence resonance energy transfer) between MDC and AO in autophagolysosomes (red fluorescence) was evaluated at excitation wavelength of 330-385 nm (U-MWU2 filter). NAO and AO were evaluated at excitation wavelength of 450-480 nm (U-MWB2 filter). MTKred fluorescence was evaluated at excitation wavelength of 510-550 nm (U-MWG2 filter).

More than 50 images at 1000x magnification per treatment were acquired. For the assessment of morphometric data, monochrome layers from RGB images were digitally separated, pseudo-coloured and segmented with ImagePro Plus 6.0. Improvement of edge detection was obtained with fast Fourier transformation (FFT) and Laplace filter. Morphometric measurements (area, roundness, perimeter, major axis, minor axis) of segmented features were exported to MS-Excel and statistical analysis was performed with GraphPad Prism 4.0. Image merging and co-localization analysis was also done with Image Pro Plus 6.0.

6- Statistical analysis

Data obtained from digital analysis of images were evaluated for differences in distribution by the non-parametric Kruskal-Wallis test, followed by Dunn's post-hoc test to check statistical significance of differences between treated samples. Two sample cases were evaluated with Mann-Whitney U test. Box-Whisker plots were obtained with Graph Pad Prism to visualize the drug-induced changes in each parameter frequency distribution.

Results

CL content, MMP and cell viability assessed through NAO *versus* TMRE / PI correlation plots

The evaluation of MMP, MM and cell death was conducted with a triple fluorescent stain (TMRE, NAO and PI, respectively) and analysis by flow cytometry. The correlation plots of NAO *versus* TMRE showed three clusters: 1) cells with high MMP and high NAO fluorescence, 2) cells with collapsed MMP and high NAO fluorescence, and 3) cells with collapsed MMP but low NAO fluorescence (Fig. 1A). The abrupt reduction of NAO fluorescence has been previously demonstrated to be caused by massive oxidation of cardiolipin [21]. Thus, we refer to low NAO fluorescence as oxCL content and high NAO fluorescence as rdCL content. The fluorescence of TMRE was detected in the parameter FL2 (590/20nm) but not in the parameter FL3 (670/20nm) as shown in Fig. 1B. When samples were stained with NAO, TMRE and PI, it occurred that PI was detected in FL2 and FL3 (Fig. 1D and 1E, upper left quadrant). However, dead cells never have a positive MMP, and thus live cells with a positive MMP and rdCL content were located in the upper right quadrant in correlation plots of NAO *versus* FL2 (Fig. 1D). In addition, the single cluster of cells with oxCL shown in the lower left quadrant of Fig. 1A was split in a cluster of live cells with oxCL content and dead cells with oxCL content (shown in lower and top left quadrants of Fig. 1D, respectively). As shown in Fig. 1E, dead cells

observed in upper left quadrant of NAO *versus* FL2, coincide with dead cells detected in NAO *versus* FL3 (PI fluorescence only). Thus, we refer to the parameter FL2 as TMRE / PI, and we present a scheme of the possible transitions of cells from one cluster to another in the correlation plot of NAO *versus* TMRE/PI fluorescence, due to factors such as cytotoxic drug treatment (Fig. 1F). This correlation plot allowed the identification of live cells with a positive MMP (cluster 1 in Fig. 1F), live cells with collapsed MMP but no evidence of oxCL (cluster 2 in Fig. 1F), live cells with collapsed MMP but oxCL (cluster 3 in Fig. 1F) and finally a cluster of dead cells (cluster 4 in Fig. 1F). We will further refer to clusters 1 to 4 in the text to interpret changes induced by drug treatment.

CCCP caused collapse of MMP and increased ROS after 30 min. but did not affect cell viability

We evaluated the short-time effect (30 min.) of increasing doses of CCCP through this correlation analysis. As expected, CCCP caused collapse of MMP but did not cause a massive oxidation of CL, as indicated by the high NAO fluorescence detected even at the highest dose of 50μM (Fig. 1G through L). There was no change in the amount of dead cells as indicated by PI staining (Fig. 1 G through L).

As expected, CCCP increased O_2^- and decreased the amount of GSH within 30 min., and the correlation analysis of NAO *versus* HE in double-stained cells showed that most of the O_2^- burst occurred in live cells with rdCL content that corresponded to clusters 1 and 2 in Fig. 1F (shown in supplemental Fig. 1).

CCCP induced mitochondrial fission

The fluorescence microscopy of NAO stained cells evaluated after 30 min. showed that CCCP treatment caused a shift from partially elongated shapes to predominantly round shapes in the mitochondrial network (Fig. 2A). These changes were quantified by digital image processing computing the roundness index (RI), a morphometric measure that approaches 1.0 in perfectly round features and sets off from 1.0 in elongated shapes (Fig. 2B). We next used subcellular flow cytometry to confirm the increase in the amount of round-shaped mitochondria. In this approach, the cell suspensions stained with NAO were ruptured by ultrasound cavitation immediately prior to flow cytometry analysis. Only particles with mitochondrial content (NAO fluorescence) were considered in the analysis (Fig. 2C). The complete rupture of cells was monitored in correlation plots to exclude intact cells and particles that laid out of the main cluster of subcellular particles (Fig. 2D).

The increase in round-shaped mitochondria was correlated to the increase in SSC-A (the area of the pulse of side scatter light generated by mitochondria-containing particles), as illustrated in Fig. 2C. The increase in the fraction of mitochondria-containing particles with high SSC-A as a function of CCCP dose is shown in Fig. 2E.

CCCP induces a dose-dependent lysosomal volume expansion and rupture with cytoplasmic acidification

Since mitophagy involves the eventual degradation in the lysosomes, we explored the changes induced by CCCP in the morphological distribution of lysosomes. Within the range 5-30 µM CCCP, we noted an increase in the area of lysosomes as indicated by AO staining and fluorescence microscopy (Fig. 3A). This lysosomal expansion was associated with lysosome rupture in many cells and complete elimination of lysosomes in other cells, particularly with doses of 30-40 µM CCCP (Fig. 3A and B). Similar results were obtained after staining with the lysosome probe neutral red (data not shown). In addition, lysosome rupture was correlated to intracellular acidification, as indicated by staining with FDA, a fluorescein-based probe that decreases fluorescence emission at low intracellular pH [26](Fig. 3C).

CCCP induced autophagosome expansion at 10µM and increased colocalization of autophagosomes and mitochondria

Cells treated with 10 µM CCCP and evaluated after 30 min. showed an increase in the amount of autophagosomes, as detected by fluorescence microscopy of MDC-stained cells (Fig. 3D and E). The increase in MDC fluorescence after CCCP treatment was confirmed by UV-excited flow cytometry (Fig. 3F). The correlation analysis of NAO *versus* MDC showed that the increase in autophagosomes occurred in live cells with rdCL content (Fig. 3F). There was also an increase in the area of co-localized mitochondria and autophagosomes in samples treated with 10µM CCCP (Fig. 3G and H).

CCCP induced an increase in autophagolysosomes as detected by MDC+AO staining

Autophagosomes were observed through the cyan fluorescence of MDC with UV excitation (Fig. 4A through D), while lysosomes were observed through red fluorescence emission of AO with blue light excitation (Fig. 4E and F), in double-stained cells. After 20-30-min. incubation with both MDC and AO, some autophagosomes showed red fluorescence with UV-light excitation. This occurred due to deliver of the probe MDC to the lysosomes and interaction with AO. This interaction resulted in decreased blue fluorescence from MDC and increased red fluorescence from AO at the sites of autophagolysosomes (Fig. 4G and H), due to occurrence of fluorescence resonance energy transfer (FRET) between MDC (donor probe) and AO (acceptor probe). The merged image of

autophagosomes and lysosomes (Fig. 4J through M) showed that co-localization areas were partially co-incident with autophagolysosomes as directly observed through red fluorescence emission with UV-light excitation (Fig. 4N through Q).

Survival of cells after 72 hr of CCCP treatment and changes in CL content and MMP

We next explored the effect of increasing doses of CCCP after 72 hr to determine the extent of tolerance to the sudden increase in mitochondrial and lysosome damage, with high levels of oxidative stress and intracellular acidification. The percentages of cells within each of the regions of the correlation plots described in Fig. 1F, observed at different CCCP doses in 72-hr assays, were plotted in line graphs (Fig. 5A). In addition, the changes in MM and MMP as indicated by NAO and TMRE fluorescence were also plotted in line graphs (Fig. 5 top). The effects were different within the 0-15-μM CCCP range (low-dose range, LDR) and 20-50 μM CCCP range (high-dose range, HDR). Within the LDR, there was an increase in MM, a decrease in cells with a positive MMP (cluster 1), an increase in cells with collapsed MMP and rdCL content (cluster 2), an increase in cells with collapsed MMP and oxCL (cluster 3), and an increase in dead cells (cluster 4) up to 20% (Fig. 5A and B). Within the HDR, there were no changes in MM, no positive MMP, an increased fraction of cells with rdCL (cluster 2), and of cells with collapsed MMP and oxCL (cluster 3), with a fraction of dead cells of about 20% (cluster 4) (Fig. 5A). The viability scored by the NAO TMRE PI triple staining was confirmed to be similar to that evaluated by the FDA PI staining method (Fig. 5C).

Drugs that block mitophagy increase MM and compromise survival after 72 hr of CCCP treatment particularly in the LDR of CCCP

Mdivi-1 is an inhibitor of Drp1, a molecule required for mitochondrial fission [28]. By blocking fission, Mdivi-1 inhibits the first step of mitophagy, apart from creating a hyperfused mitochondrial network. This effect was confirmed by fluorescence microscopy of cells treated with 50 μM Mdivi-1 and stained with MDC and mitotracker (Fig. 6C). When cells were co-treated with CCCP and Mdivi-1, we observed an increase in MM with increased cell death, particularly over the LDR (cluster 4). There was also a decrease of cells with a positive MMP (cluster 1), and of cells with collapsed MMP and rdCL content (cluster 2), with increased amount of live cells with oxCL (cluster 3) (Fig. 6A and B). The co-treatment of cells with CCCP and 1μM VCR (an inhibitor of autophagosome transport) also increased MM, decreased cells with a positive MMP and increased dead cells, particularly in the LDR (clusters 1 and 4, respectively). Similar to Mdivi-1, VCR decreased the amount of cells in cluster 2 and increased cells in cluster 3 (Supplemental Figure 2).

Drugs influencing mitochondrial biogenesis and the unfolded protein response differentially compromised cell survival after 72 hr of CCCP

The occurrence of lysosomal damage within the HDR of CCCP excluded mitophagy as a relevant stress response for cell survival after massive mitochondrial damage, since lysosomes are indispensable for mitophagy and autophagy. Co-treatment with CCCP and 1mM VPA, a drug that induces mitochondrial biogenesis, only increased MM within the LDR but decreased survival of cells after 72 hr (Fig. 7A). Doxycycline disrupts mitochondrial biogenesis by altering mitochondrial protein import [29, 30]. Co-treatment with 10 μM Doxycycline and CCCP slightly decreased MM within the LDR of CCCP, but had a negligible effect in cell survival when compared to cells treated only with CCCP (Supplemental Figure 3). The proteasome can have a critical role in the absence of mitophagy to restore mitochondrial function. In contrast to inhibitors of mitophagy, MG132 increased cell death only in the HDR of CCCP (Fig. 7B). In addition, co-treatment with MG132 decreased MM at the LDR and the HDR, decreased the amount of cells in cluster 2 within the HDR, and had no effect on the amount of cells in clusters 1 and 3 at any of the CCCP doses evaluated (Fig. 7B). The inhibitor of glycolysis IAA [31] had an influence only in the HDR of CCCP with increased cell death (cluster 4), decreased cells in cluster 2 and increased cells in cluster 3 (Supplemental Figure 3).

Discussion

Mitochondrial destabilization as a drug target has been considered an auspicious approach to cancer treatment [32]. The renewed interest in uncouplers for the treatment of several diseases associated with alterations in mitochondrial function, including cancer, has fostered the recent development of new uncouplers with improved therapeutic index [8]. The mechanism of damage by collapse of the MMP and mitochondrial failure is shared by almost all cytotoxic drugs that target mitochondria, and pro-survival cell stress responses that oppose the effect of uncouplers like CCCP may be involved in resistance to other mitocans as well [6]. Although collapse of MMP is often considered the first step in mitochondrial apoptosis, as shown in the present study CCCP caused MMP collapse within 30 min. in the Burkitt's lymphoma cell line Raji, but less than 20% of cells were dead after 72 hr. Therefore, MMP collapse and massive oxidative stress, with widespread cellular damage, lysosome destabilization and intracellular acidification, was not enough to trigger mitochondrial apoptosis and cell death in the majority of CCCP-treated cells. In the context of RCD, this result raises the intriguing question of what cellular stress responses could be behind the high tolerance to such a widespread cellular damage cause by CCCP. In some cases, aggressive cancer cells may be dependent on

particular stress response, and inhibition of such dominant stress response could be lethal for cancer cell survival. The high potency of proteasome inhibitors in multiple myeloma cells is often cited as a leading example of this concept. Myeloma cells are highly dependent on the ubiquitin proteasome system (UPS), and proteasome inhibitors induce endoplasmic reticulum stress and cell death [33]. However, it is also possible that many kinds of cell stress responses could operate at the same time and even have differential predominance depending on the extent of mitochondrial and cellular damage.

Mitophagy was the main candidate to support survival after CCCP treatment, because it could aid in elimination of the root cause of cell damage, i.e. the faulty mitochondria. However, mitophagy requires functional lysosomes, and massive lysosomal destabilization and rupture excludes a protecting role of mitophagy in the HDR of CCCP treatment. The inhibitors of mitophagy Mdivi-1 and VCR increased cell death within the LDR, suggesting that mitophagy as a protective cell stress response still had a role within the LDR of CCCP treatment. Many other features of active mitophagy and autophagy were present within the LDR of CCCP, such as expansion of autophagosomes, autolysosomes and colocalization between autophagosomes and mitochondria. Mdivi-1 and VCR increased MM, particularly over the LDR, confirming that inhibition of mitophagy led to accumulation of mitochondria. In addition, decreased amount of cells with positive MMP (cluster 1), decreased live cells with collapsed MMP and rdCL content (cluster 2), increased live cells with collapsed MMP and oxCL (cluster 3), were all changes consistent with increased mitochondrial damage and increased cell death (cluster 4) after inhibition of mitophagy within the LDR.

Mdivi-1 but not VCR increased cell death due to CCCP in the HDR. This could be due to the possible adverse effect of hyperfusion with uncoupling of the ETC and extensive mitochondrial damage. Thus, mitophagy could be the predominant stress response within the LDR of CCCP but not in the HDR.

Under lysosomal destabilization as occurred within the HDR, the biogenesis of new mitochondria could operate as a compensating pro-survival response. However, VPA increased MM only within the LDR, and in fact, it increased cell death. Within the HDR, VPA had only a marginal effect, and almost no influence on cell death rates caused by CCCP. Doxycycline, an antibiotic that disrupts mitochondrial biogenesis [29], decreased MM within the LDR but had no effect on survival rates from CCCP treatment.

The UPS could have a compensating role as part of the unfolded protein cell stress response when mitophagy and autophagy are halted, as occurred in the HDR of CCCP [34]. The UPS is an active part of an alternative mitochondrial quality control process known as outer mitochondrial membrane-

associated degradation (OMMAD)[35]. Consistent with this notion, the proteasome inhibitor MG132 increased cell death and decreased cells in cluster 2, only within the HDR of CCCP treatment. The widespread mitochondrial damage within the HDR of CCCP would create a demand for enhanced glycolysis. This could explain the enhanced cell death that we observed with the inhibitor of glycolysis IAA over the HDR of CCCP [36]. Thus, several stress responses including mainly the UPS and metabolic reprogramming, may operate concurrently within the HDR of CCCP to support survival and avoid RCD in lymphoma cells. The assessment of differential predominance of cell stress responses after incremental mitochondrial damage, may contribute to the design of combinations of targeted cytotoxic drugs. The threshold to initiate RCD may be lowered by targeting these stress responses. In particular, drugs that destabilize lysosomes may block mitophagy and synergize with proteasome inhibitors and drugs that initiate mitochondrial apoptosis.

Figure legends

Figure 1

Effect of CCCP in Raji cells after 30-min. treatment. Raji cells treated with 10 µM CCCP for 72 hr were stained with NAO and TMRE (A through C). Panel B shows that no TMRE fluorescence was detected in FL3 channel (630nm fluorescence detector). Panel C shows the size (FSC) and granularity (SSC) of CCCP-treated cells. Panels D through F show a replicate sample stained with NAO, TMRE and PI. Dead cells appear as a cluster in top left quadrants in panels D and E (PI positive, indicating loss of plasma membrane selectivity). Dead cells always show oxCL content and can never have a positive MMP. Thus, the clusters in upper left and upper right quadrant correspond to mutually exclusive categories of cells. Panel F illustrates the possible transitions of cells between clusters due to drug treatment and cell stress responses. Panels G through L show that after 30 min., CCCP caused collapse of MMP but not cell death, as indicated by the percentages in cluster 4 (Q1). Most cells appeared with rdCL content, and a very low fraction had oxCL content as indicated by clusters 2 and 3, respectively (following the scheme of panel F). One experiment representative of four.

Figure 1

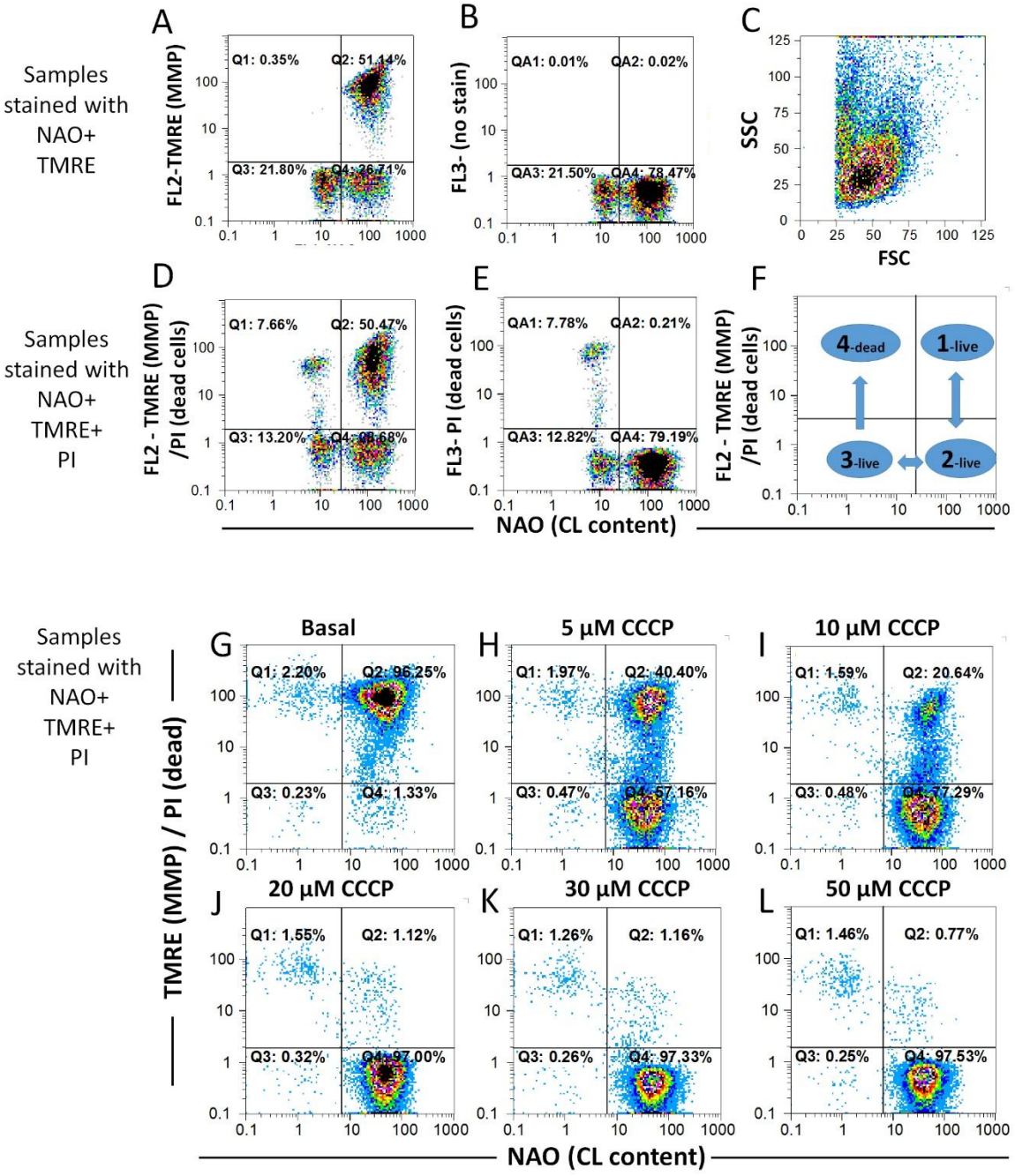

Figure 2

CCCP treatment changes mitochondrial morphology after 30 min.

A) Fluorescence microscopy of CCCP-treated cells stained with NAO showing fragmentation and rounding of the mitochondrial network (mitochondrial fission). Several images were digitally segmented (illustrated in small panels at the right side), to compute the roundness index (RI). This index approaches 1.0 in round-shaped mitochondria (predominance of mitochondrial fission). Size bar = 5 µm.

B) Cells treated with 10 µM CCCP had decreased RI. Error bars indicate SE of the mean. P-value < 0.001 for CCCP *versus* Basal (N=430.)

C) Evaluation of fission by subcellular flow cytometry. Cells were stained with NAO and ruptured by ultrasound cavitation immediately prior to flow cytometry analysis. Only particles with NAO fluorescence (mitochondria containing particles) were acquired. The parameter SSC-A (the area of the pulse detected from each particle) was correlated to the roundness of mitochondria as detected in fluorescence microscopy.

D) The upper plot shows the region R2 of big mitochondria-containing particles with high NAO content that corresponded to non-ruptured cells that were excluded from analysis. The lower panel shows the region R1 that encloses the size-range of mitochondria-containing particles included in the analysis.

E) The proportion of cells with high SSC-A (predominance of fission) was increased after 30 min. of CCCP treatment. More than 40,000 mitochondria-containing particles were analysed in each sample. Bars indicate mean value ± SE of triplicates. One experiment representative of three.

Figure 2

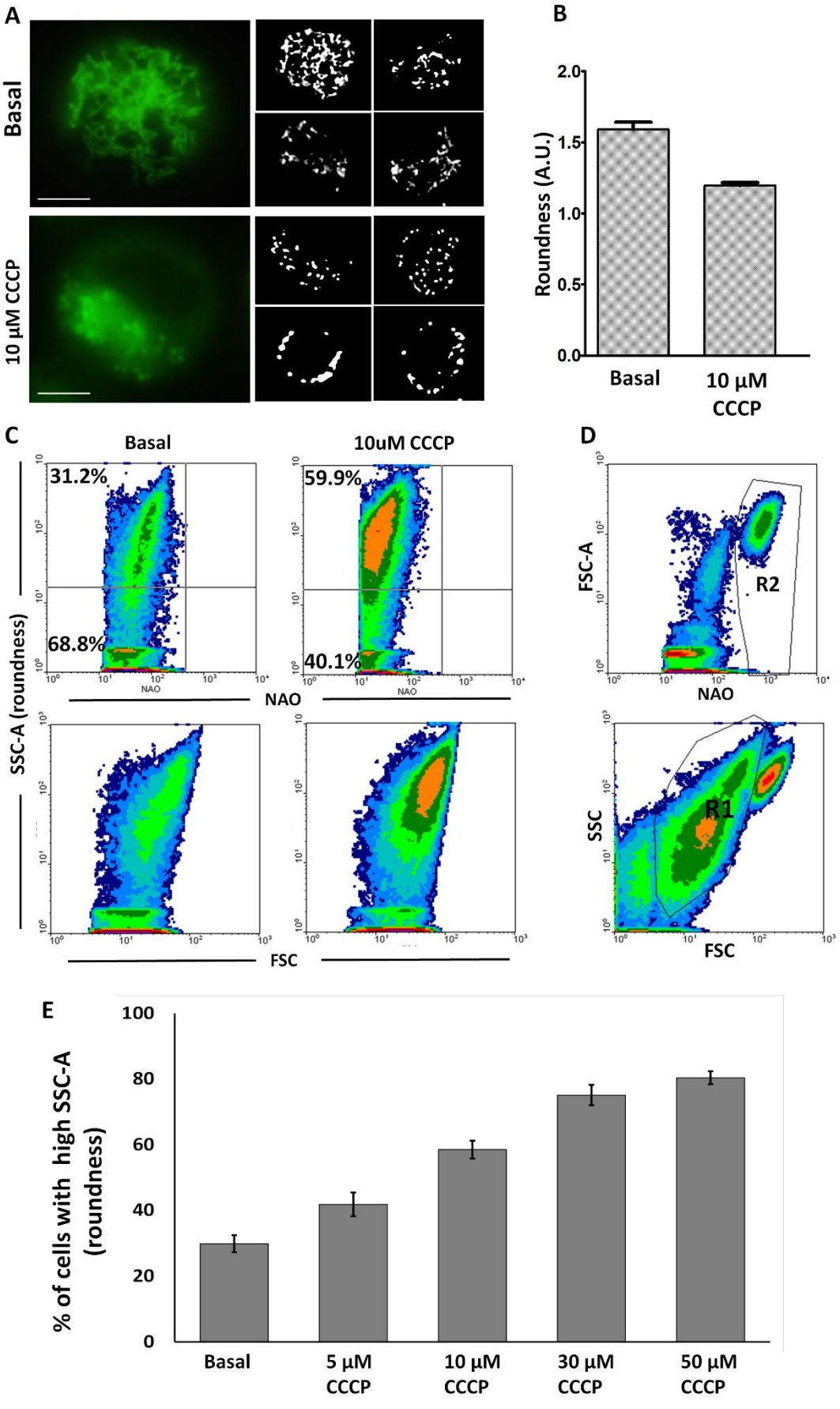

Figure 3

CCCP treatment increased lysosomes and autophagosomes after 30 min.

A) Lysosome volume was massively expanded with increasing doses of CCCP (white arrows). At high CCCP doses, the entire cytoplasm (often including the nucleoli) was often stained as an acid compartment (arrow head), although many cells were seen completely depleted of lysosomes (red arrows). Size bar = 10 µm.

B) Box-Whisker plots showing median, quartiles and extreme values of the ratio of lysosomal area/cell area (computed from several digital images) and illustrating the lysosomal expansion, as well as the decline at higher doses due to lysosomal rupture.

C) Change in the intracellular pH as indicated by mean fluorescence intensity (MFI) of FDA. Bars indicate ± SE of the MFI. CCCP doses were assayed in triplicates. One experiment representative of three. The dotted line corresponds to a polynomial approximation of MFI values. The histogram illustrates a basal sample (grey-shaded area) and a 10-µM CCCP-treated sample (line).

D) Cells were stained with MDC showing the increase in autophagosomes. Size bar = 10 µm.

E) Box Whisker plot showing a comparison of the ratio of autophagosome area / cell area ($P < 0.001$ for comparison between CCCP treated *versus* basal sample in Mann-Whitney U-test).

F) Increase in autophagosomes detected in flow cytometry analysis of MDC-stained cells. The increase in autophagosomes occurred in cells with rdCL content. The RN1 region corresponds to the proportion of cells with high content of autophagosomes. One experiment representative of three.

G) Mitochondrial network stained with NAO shown in pseudo-colour green, autophagosomes stained with MDC in pseudo-colour red, showing the increase in co-localization between mitochondria and autophagosomes (yellow). Size bar = 10 µm.

H) Area of mitochondria (green), autophagosomes (red) and co-localized mitochondria and autophagosomes (yellow), scored in single cells. The bar graph illustrates the expansion of autophagosomes and the increase of mitochondria co-localized with autophagosomes. A.U. arbitrary units

Figure 3

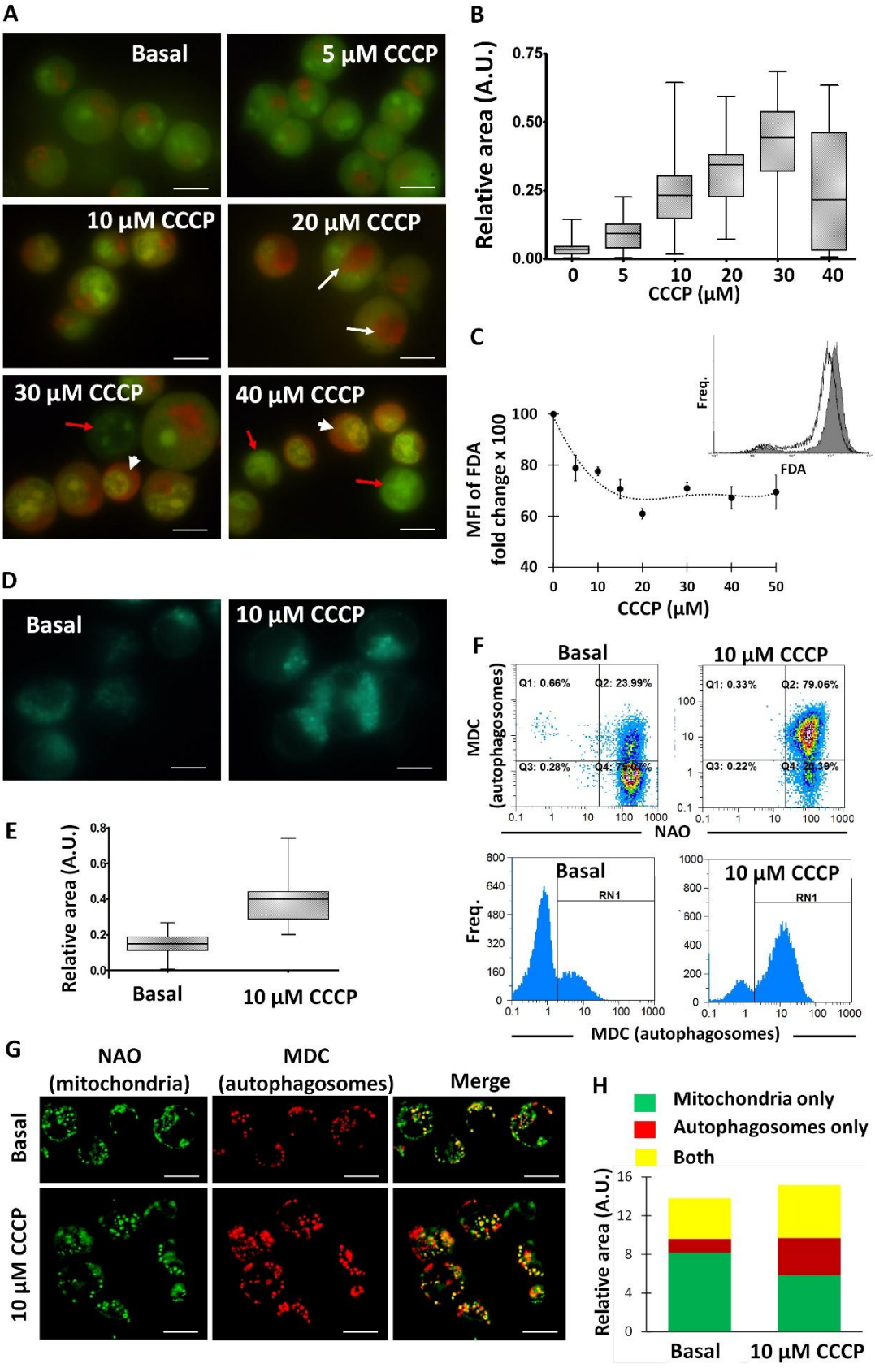

Figure 4

CCCP increased autophagolysosomes after 30 min.

Basal and 10µM CCCP treated cells were stained with MDC and AO. Autophagosomes (Autoph) were detected as cyan fluorescent with UV light excitation (A and B original images, C and D segmented images with pseudo-colour), and lysosomes(Lys) were detected as red fluorescent with blue light excitation (E and F). After 20 min. of incubation with MDC + AO, a number of autophagosomes became red fluorescent with UV-light excitation, due to the fusion of autophagosomes and lysosomes and the occurrence of FRET between MDC and AO. The image of these autophagolysosomes (AutopLys) was digitally segmented and is shown in pseudo-colour magenta (panels G and H). The area of autophagolysosomes was increased in samples treated with 10 µM CCCP (panel H). Merge image of autophagosomes and lysosomes also showed an increase in the area of co-localization with CCCP treatment (panels J through M). Merge image of autophagosomes (cyan), lysosomes (red) and autophagolysosomes (magenta) illustrated the spatial relationship between these vesicles after expansion with CCCP treatment (N through Q). Size bar = 10 µm

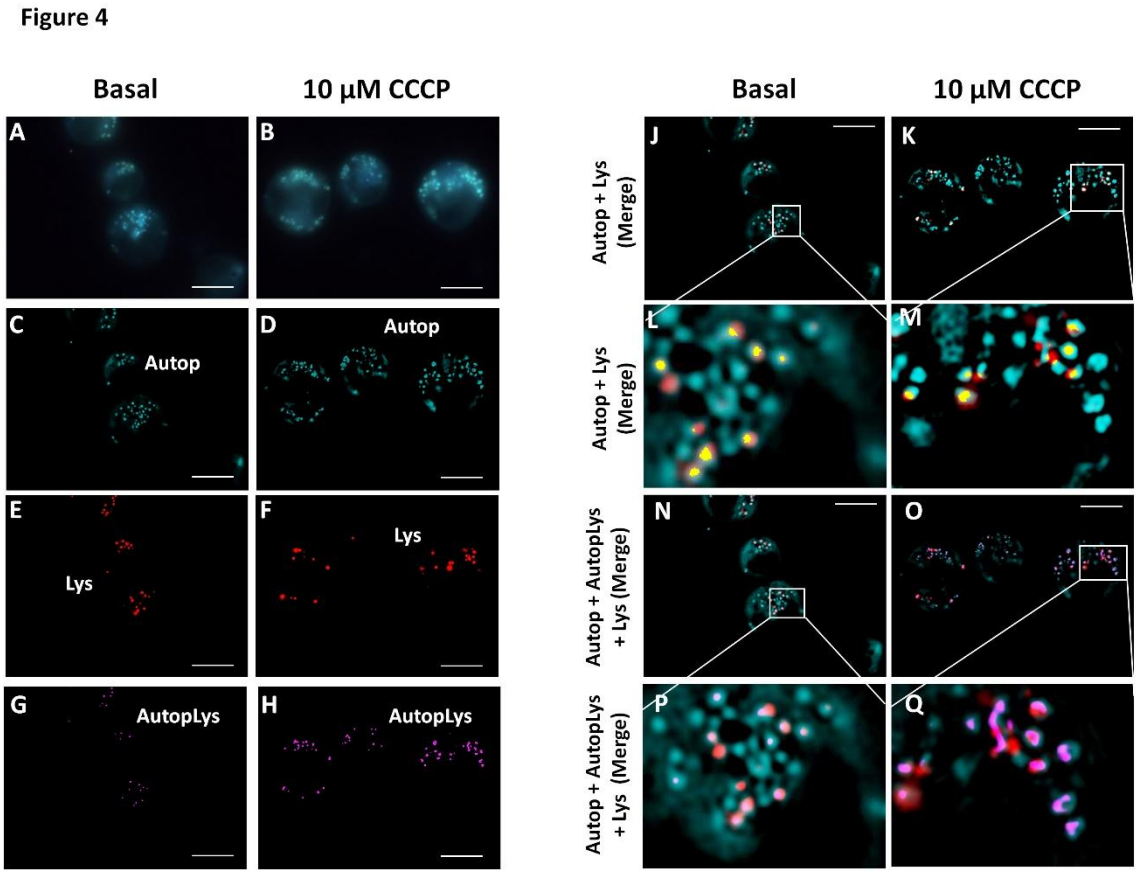

Figure 5

Cell survival after 72 hr of CCCP treatment

A) Line graphs created with percentage and MFI values from correlation plots of NAO *versus* TMRE/PI considering the four quadrants mentioned in the scheme of Fig. 1F. Mitochondrial mass was increased within the range 0-15 µM CCCP (top left). Only cells exposed to less than 15 µM had a positive MMP (top and mid right). Within the range 0-15 µM CCCP, there was an increase in cells with rdCL content and collapsed MMP (low right). There was an increase in cells with oxCL and collapsed MMP (left bottom). The number of dead cells increased within the range 0-15 µM but was unchanged within the range 20-50µM (mid left). Bars indicate ± SE of the mean of five experiments.

B) Representative correlation plots of NAO *versus* TMRE/PI fluorescence within the 0-15-µM CCCP dose range. The increase in CCCP dose caused a transition of cells between quadrants as indicated in the scheme of Fig. 1F.

C) Bar graph showing that the scoring of dead cells by flow cytometry using FDA PI was similar to the scoring of dead cells stained with NAO TMRE PI. Bars indicate ± SE of the mean from triplicates. One experiment representative of three.

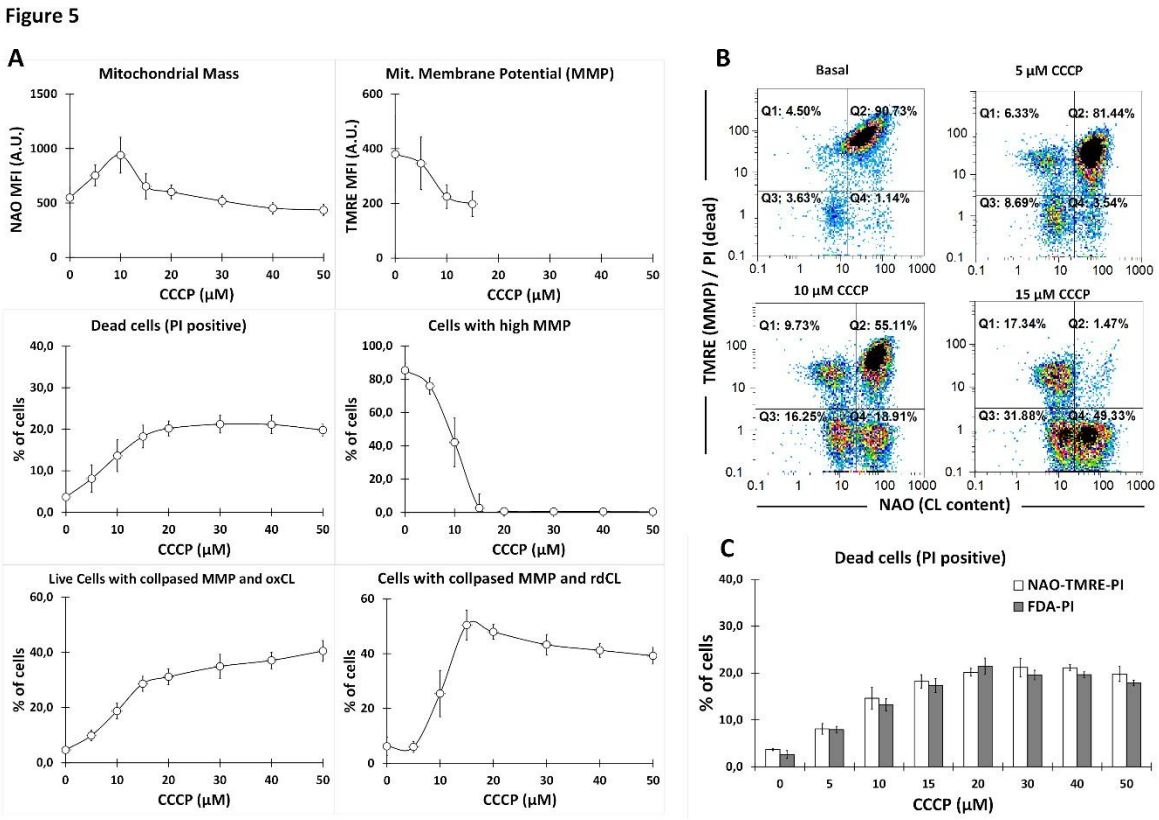

Figure 6

Mdivi-1 created a hyperfused mitochondrial network, increased MM and decreased cell survival after CCCP treatment

A) Line graphs created with percentage and MFI values from correlation plots of NAO *versus* TMRE/PI fluorescence, considering the four quadrants indicated in Fig. 1F. Mdivi-1 increased MM over the whole dose range evaluated, decreased cells with collapsed MMP and rdCL content, increased live cells with oxCL and increased dead cells. Mean values from triplicates. One experiment representative of three.

B) Representative correlation plots of NAO *versus* TMRE/PI fluorescence from samples treated with 5µM CCCP and 5µM CCCP + 50 µM Mdivi-1.

C) Fluorescence microscopy of cells treated with Mdivi-1 showing a hyperfused mitochondrial network with almost no co-localization with autophagosomes. Samples were stained with MDC and mitotracker (pseudo-colour green and red, respectively, applied to black and white images). Size bar = 5 µm.

Figure 6

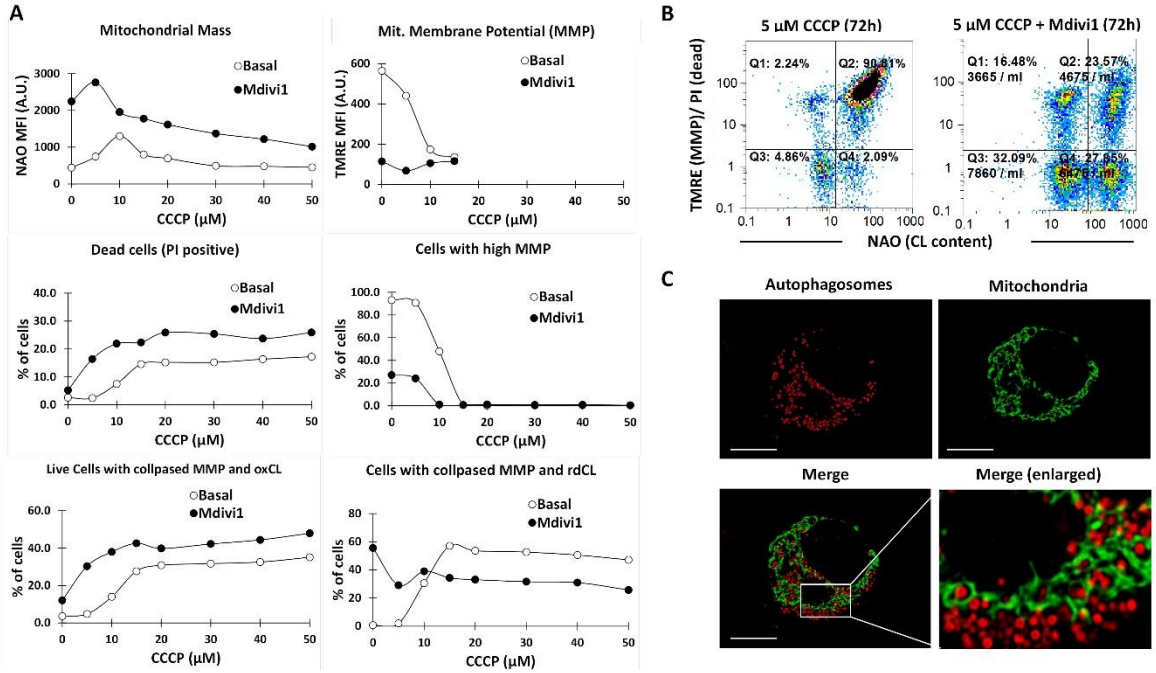

Figure 7

Effects of increased mitochondrial biogenesis and inhibition of the proteasome on cell survival after CCCP treatment

Line graphs created with percentages and MFI values from correlation plots of NAO *versus* TMRE/PI, considering the four quadrants described in the scheme of Fig. 1F. The effect of 1mM VPA (increased mitochondrial biogenesis) and 400 nM MG132 (inhibition of the proteasome) over cells treated with CCCP are shown in panels A and B, respectively. Mean values from triplicates. One experiment representative of three.

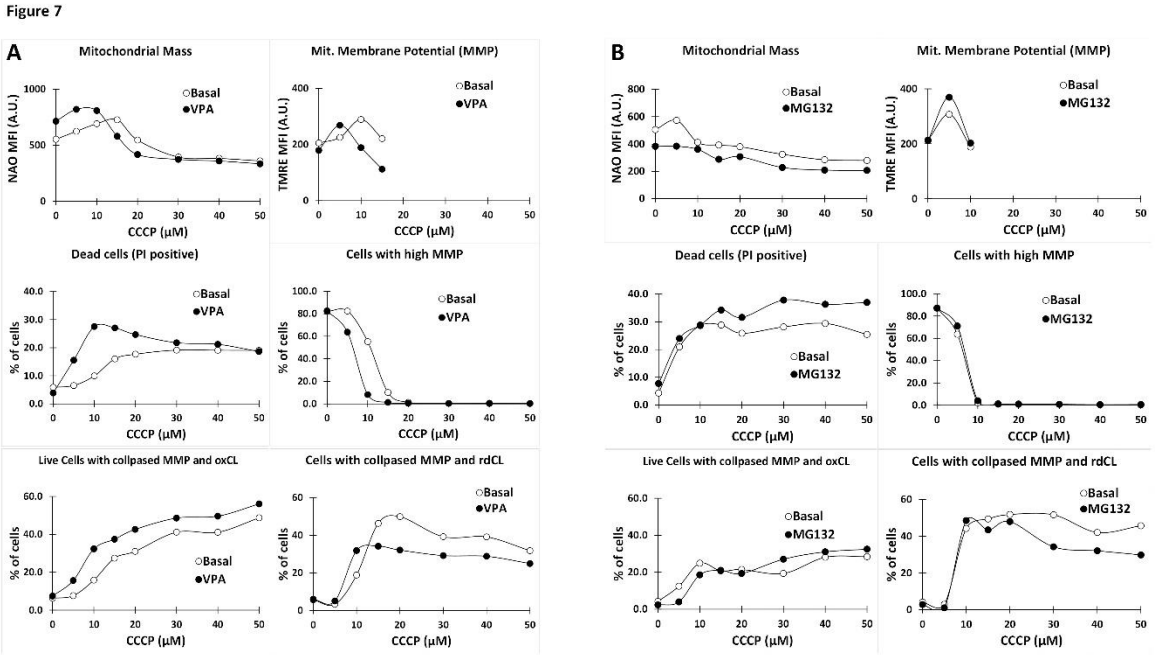

Acknowledgements

We thank Laboratorio Filaxis for providing us with Vincristine. This work was supported with grants 20720120200016BA from SECYT-UBA and grant PIP 11220090100199 from CONICET.

Conflict of interests

Authors declare no conflict of interests.

References

1. Galluzzi L, Bravo-San Pedro JM, Kepp O, Kroemer G. Regulated cell death and adaptive stress responses. Cellular and molecular life sciences : CMLS. 2016;73:2405-10.
2. Galluzzi L, Bravo-San Pedro JM, Vitale I, Aaronson SA, Abrams JM, Adam D, et al. Essential versus accessory aspects of cell death: recommendations of the NCCD 2015. Cell death and differentiation. 2015;22:58-73.
3. Tait SW, Green DR. Mitochondria and cell death: outer membrane permeabilization and beyond. Nature reviews Molecular cell biology. 2010;11:621-32.
4. Madesh M, Hajnoczky G. VDAC-dependent permeabilization of the outer mitochondrial membrane by superoxide induces rapid and massive cytochrome c release. The Journal of cell biology. 2001;155:1003-15.
5. Paradies G, Paradies V, Ruggiero FM, Petrosillo G. Cardiolipin and mitochondrial function in health and disease. Antioxidants & redox signaling. 2014;20:1925-53.
6. Neuzil J, Dong LF, Rohlena J, Truksa J, Ralph SJ. Classification of mitocans, anti-cancer drugs acting on mitochondria. Mitochondrion. 2013;13:199-208.
7. Park JS, Kang DH, Bae SH. p62 prevents carbonyl cyanide m-chlorophenyl hydrazine (CCCP)-induced apoptotic cell death by activating Nrf2. Biochemical and biophysical research communications. 2015;464:1139-44.
8. Shikata Y, Kiga M, Futamura Y, Aono H, Inoue H, Kawada M, et al. Mitochondrial uncoupler exerts a synthetic lethal effect against beta-catenin mutant tumor cells. Cancer science. 2017;108:772-84.
9. Galluzzi L, Kepp O, Kroemer G. Mitochondria: master regulators of danger signalling. Nature reviews Molecular cell biology. 2012;13:780-8.
10. Kornblihtt L, Carreras M, Blanco G. Targeting mitophagy in combined therapies of haematological malignancies. Gorbunov N, editor. Rijeka, Croatia: Intech Open Publisher 2016.
11. Ney PA. Mitochondrial autophagy: Origins, significance, and role of BNIP3 and NIX. Biochimica et biophysica acta. 2015;1853:2775-83.
12. Chu CT, Ji J, Dagda RK, Jiang JF, Tyurina YY, Kapralov AA, et al. Cardiolipin externalization to the outer mitochondrial membrane acts as an elimination signal for mitophagy in neuronal cells. Nature cell biology. 2013;15:1197-205.
13. Cavaliere V, Lombardo T, Costantino SN, Kornblihtt L, Alvarez EM, Blanco GA. Synergism of arsenic trioxide and MG132 in Raji cells attained by targeting BNIP3, autophagy, and mitochondria with low doses of valproic acid and vincristine. Eur J Cancer. 2014;50:3243-61.
14. Twig G, Elorza A, Molina AJ, Mohamed H, Wikstrom JD, Walzer G, et al. Fission and selective fusion govern mitochondrial segregation and elimination by autophagy. The EMBO journal. 2008;27:433-46.

15. Mackeh R, Perdiz D, Lorin S, Codogno P, Pous C. Autophagy and microtubules - new story, old players. Journal of cell science. 2013;126:1071-80.
16. Stotland A, Gottlieb RA. Mitochondrial quality control: Easy come, easy go. Biochimica et biophysica acta. 2015;1853:2802-11.
17. Jazwinski SM. The retrograde response: when mitochondrial quality control is not enough. Biochimica et biophysica acta. 2013;1833:400-9.
18. Sitarz KS, Elliott HR, Karaman BS, Relton C, Chinnery PF, Horvath R. Valproic acid triggers increased mitochondrial biogenesis in POLG-deficient fibroblasts. Molecular genetics and metabolism. 2014;112:57-63.
19. Yoon JY, Ishdorj G, Graham BA, Johnston JB, Gibson SB. Valproic acid enhances fludarabine-induced apoptosis mediated by ROS and involving decreased AKT and ATM activation in B-cell-lymphoid neoplastic cells. Apoptosis : an international journal on programmed cell death. 2014;19:191-200.
20. Ward PS, Thompson CB. Metabolic reprogramming: a cancer hallmark even warburg did not anticipate. Cancer cell. 2012;21:297-308.
21. Li XX, Tsoi B, Li YF, Kurihara H, He RR. Cardiolipin and its different properties in mitophagy and apoptosis. The journal of histochemistry and cytochemistry : official journal of the Histochemistry Society. 2015;63:301-11.
22. Mileykovskaya E, Dowhan W, Birke RL, Zheng D, Lutterodt L, Haines TH. Cardiolipin binds nonyl acridine orange by aggregating the dye at exposed hydrophobic domains on bilayer surfaces. FEBS letters. 2001;507:187-90.
23. Jensen SS, Petterson SA, Halle B, Aaberg-Jessen C, Kristensen BW. Effects of the lysosomal destabilizing drug siramesine on glioblastoma in vitro and in vivo. BMC cancer. 2017;17:178.
24. Lombardo T, Cavaliere V, Costantino SN, Kornblihtt L, Alvarez EM, Blanco GA. Synergism between arsenite and proteasome inhibitor MG132 over cell death in myeloid leukaemic cells U937 and the induction of low levels of intracellular superoxide anion. Toxicol Appl Pharmacol. 2012;258:351-66.
25. Lombardo T, Anaya L, Kornblihtt L, Blanco G. Median Effect Dose and Combination Index Analysis of Cytotoxic Drugs Using Flow Cytometry. Schmid I, editor. Rijeka, Croatia: Intech Open Publisher 2012.
26. Visser JW, Jongeling AA, Tanke HJ. Intracellular pH-determination by fluorescence measurements. The journal of histochemistry and cytochemistry : official journal of the Histochemistry Society. 1979;27:32-5.
27. Degtyarev M, Reichelt M, Lin K. Novel quantitative autophagy analysis by organelle flow cytometry after cell sonication. PloS one. 2014;9:e87707.
28. Wu Q, Xia SX, Li QQ, Gao Y, Shen X, Ma L, et al. Mitochondrial division inhibitor 1 (Mdivi-1) offers neuroprotection through diminishing cell death and improving functional outcome in a mouse model of traumatic brain injury. Brain research. 2016;1630:134-43.
29. De Luca A, Fiorillo M, Peiris-Pages M, Ozsvari B, Smith DL, Sanchez-Alvarez R, et al. Mitochondrial biogenesis is required for the anchorage-independent survival and propagation of stem-like cancer cells. Oncotarget. 2015;6:14777-95.
30. Moullan N, Mouchiroud L, Wang X, Ryu D, Williams EG, Mottis A, et al. Tetracyclines Disturb Mitochondrial Function across Eukaryotic Models: A Call for Caution in Biomedical Research. Cell reports. 2015.
31. Schmidt MM, Dringen R. Differential effects of iodoacetamide and iodoacetate on glycolysis and glutathione metabolism of cultured astrocytes. Frontiers in neuroenergetics. 2009;1:1.
32. Fulda S, Galluzzi L, Kroemer G. Targeting mitochondria for cancer therapy. Nature reviews Drug discovery. 2010;9:447-64.
33. Vincenz L, Jager R, O'Dwyer M, Samali A. Endoplasmic reticulum stress and the unfolded protein response: targeting the Achilles heel of multiple myeloma. Molecular cancer therapeutics. 2013;12:831-43.

34. Pellegrino MW, Nargund AM, Haynes CM. Signaling the mitochondrial unfolded protein response. Biochimica et biophysica acta. 2013;1833:410-6.
35. Neutzner A, Benard G, Youle RJ, Karbowski M. Role of the ubiquitin conjugation system in the maintenance of mitochondrial homeostasis. Annals of the New York Academy of Sciences. 2008;1147:242-53.
36. DeBerardinis RJ, Mancuso A, Daikhin E, Nissim I, Yudkoff M, Wehrli S, et al. Beyond aerobic glycolysis: transformed cells can engage in glutamine metabolism that exceeds the requirement for protein and nucleotide synthesis. Proceedings of the National Academy of Sciences of the United States of America. 2007;104:19345-50.